Biogeochemical properties and transports in the North East Atlantic.

Clare Johnson[1], Neil Fraser[1], Stuart Cunningham[1], Kristin Burmeister[1], Sam Jones[1], Lewis Drysdale[1], Richard Abell[1], Peter Brown[2], Estelle Dumont[1], Alan Fox[1], N. Penny Holliday[2], Mark Inall[1] and Sarah Reed[1,3]

[1]Scottish Association for Marine Science, Oban, Argyll, Scotland, PA37 1QA. [2]National Oceanography Centre, European Way, Southampton, UK, SO14 3ZH. [3]Current address: SEN Transmission, SSE, Henderson Road, Inverness, IV1 1SN.

Corresponding author: Clare Johnson (clare.johnson@sams.ac.uk)

Key Points:

- Silicate decreases and pH and oxygen increase from April to May with oxygen and pH showing a secondary peak in October.
- Nutrient and carbon transports through the eastern boundary of the subpolar North Atlantic are northward and highly variable.
- Biogeochemical transport magnitude may vary on multi-annual timescales and have downstream impacts.

Abstract

The eastern subpolar North Atlantic is a source of nutrients to the Northwest European Shelf and Arctic; however, biogeochemical transports in this important region are unknown. We examine variability in nutrients and carbon at the eastern boundary of the subpolar North Atlantic between 2017-2020, and calculate their transport by a branch of the North Atlantic Current and the European Slope Current. By combining observations from moorings and ship-based surveys, we derive novel biogeochemical property transports at high temporal resolution. Data from 63 m provide new evidence of a strong seasonal signal with silicate declining between April and May (-2.3 μmol kg^{-1}) and a concurrent increase in pH (0.04) and oxygen saturation (3.5 %). Additionally, pH and oxygen saturation show a secondary peak in October during the autumn bloom. Biogeochemical transports are northwards and highly variable with volume transport dominating the variability over a multi-annual timescale. However, historical data suggests that nitrate and phosphate transports were 15 % and 19 % lower respectively in the late 2000's when the subpolar gyre circulation was weaker and lower nutrient source waters were dominant. These changes may have been amplified by concurrent reductions in volume transport. Changes in carbon and nutrient transports in the eastern subpolar North Atlantic may propagate downstream with potential effects on the Northwest European Shelf and Eurasian Arctic.

Plain Language Summary

Water flowing northward in the eastern subpolar North Atlantic transports nutrients onto the Northwest European Shelf and to the Arctic Ocean. However, biogeochemical transports through the region remain unknown. We examine variability in nutrients and carbon at the eastern boundary of the subpolar North Atlantic and calculate their transport by two important northward flowing currents. We use observations from ship-based surveys and instruments that recorded conditions in the ocean over three years to derive biogeochemical transports every 12 hours between May 2017 and October 2020. Transports of nutrients and carbon in the eastern subpolar North Atlantic are northwards although the transport is highly variable. Historical data suggests that when circulation around the subpolar North Atlantic is weaker, nutrient transports are around 15-20 % lower due to changes in the water nutrient concentrations. These changes may be amplified by concurrent reductions in current strength and volume transport. Changes in carbon and nutrient transports in the eastern subpolar North Atlantic may propagate downstream with potential effects on the Northwest European Shelf and Arctic Ocean.

1 Introduction

The Atlantic Meridional Overturning Circulation (AMOC) transports biogeochemical properties as well as mass, heat and freshwater. Whilst the Overturning in the Subpolar North Atlantic Programme (OSNAP) has examined the physical transports [e.g. *Lozier et al.*, 2019], nutrient and carbon transports at this latitude have yet to be examined. Within the North Atlantic, biogeochemical studies have focussed on the subtropics [e.g. *Brown et al.*, 2021; *Carracedo et al.*, 2021; *Lavin et al.*, 2003; *Williams et al.*, 2011], a hydrographic section between Greenland and Portugal [e.g. *Alvarez et al.*, 2004; *Fontela et al.*, 2019; *Zunino et al.*, 2015] which covers the intergyre region at its eastern reaches, and using mean velocities and nutrient climatologies at the Greenland-Scotland Ridge [*Fontela et al.*, 2019; *Maze et al.*, 2012]. Thus, although the eastern subpolar North Atlantic is an important gateway region between the high nutrient transport of the Gulf Stream [*Pelegrí and Csanady*, 1991; *Williams et al.*, 2011], and the Northwest European Shelf and Arctic Ocean, the magnitude and variability of biogeochemical transports through the region are unknown.

The Northwest European Shelf plays an important role in carbon sequestration through the shelf sea carbon pump, part of which is driven by primary productivity [e.g. *Thomas et al.*, 2004]. Upper waters in the eastern subpolar North Atlantic are an important source of nutrients to the Northwest European Shelf [*Porter et al.*, 2018; *Proctor et al.*, 1993] helping to sustain this biological activity. Changes in oceanic nutrients are a first order factor in determining levels of primary productivity on the shelf on 5-10 year timescales [*Holt et al.*, 2012], with variations in the on-shelf nutrient supply affecting the carbon cycle through changes in the biological component of the carbon pump [*Chaichana et al.*, 2019; *Humphreys et al.*, 2019]. Additionally, the influx of oceanic nutrients onto the shelf has been shown to affect the pelagic food web [*Heath and Beare*, 2008]. Although strong local variability in cross-slope transport mechanisms may dominate at some locations [*Huthnance et al.*, 2022; *Jones et al.*, 2020; *Pätsch et al.*, 2020; *Wei et al.*, in press], changes in oceanic properties are known to be communicated to the Northwest European Shelf [*Jones et al.*, 2018; *Koul et al.*, 2019]. A change in open-ocean biogeochemical concentrations directly affects the amount of nutrients available to exchange with the shelf.

Downstream of the eastern subpolar North Atlantic, Atlantic Water carried in the upper limb of the AMOC is a source of nutrients to the Arctic Ocean [*Torres-Valdés et al.*, 2013]. In particular, it supports the high primary productivity and associated carbon uptake in the Barents Sea [e.g. *Juranek*, 2022; *Wassmann et al.*, 2006]. Over the past two decades, primary productivity in the Arctic has increased with the largest changes seen on the inflow shelves including the Barents Sea [*K M Lewis et al.*, 2020]. This is likely due to increased nutrient availability, whether because of increased advection of high-nutrient Atlantic Water into the region (Atlantification), or local processes bringing more of these nutrients from the Atlantic Water reservoir to the surface. However, nitrate and phosphate concentrations within the Atlantic Water in the Eurasian Arctic declined between 1995 and 2018 [*Tuerena et al.*, 2022]. Decreases in Atlantic Water nutrient concentrations have also been observed upstream at the entrance to the Barents Sea [*Oziel et al.*, 2017; *Rey*, 2012], in the western Nordic Seas [*Rey*, 2012] and ultimately in the eastern subpolar North Atlantic [*Hátún et al.*, 2017; *C. Johnson et al.*, 2013]. These declines are thought to partly result from variations in the strength and extent of the North Atlantic subpolar gyre and associated changes in water mass distributions [*Fransner et al.*, 2023; *C. Johnson et al.*,

2013; *Rey*, 2012], with local processes also being important in the Barents Sea [*Oziel et al.*, 2017; *Tuerena et al.*, 2022] particularly in the northern polar domain [*Fransner et al.*, 2023]. When the North Atlantic subpolar gyre is energetic, subpolar-origin water masses which have relatively high nutrient concentrations influence the eastern subpolar North Atlantic. In contrast, when the subpolar gyre is weaker, water masses that originate from the subtropics or inter-gyre region with lower nutrient loadings dominate [*C. Johnson et al.*, 2013]. Other processes within the subpolar North Atlantic, such as the depth of winter convection, are also thought to play a role in the silicate decline [*Hátún et al.*, 2017]. It is hypothesised that these observed decreases in nutrient concentrations may impact and ultimately limit future Arctic primary productivity [*Oziel et al.*, 2017; *Tuerena et al.*, 2022] with knock-on effects for carbon sequestration, ecosystems and fisheries, as well as the food security of Arctic communities [*Rey*, 2012; *Tuerena et al.*, 2022]. Thus, investigating the magnitude, variability, and trends of biogeochemical transports upstream in the eastern subpolar North Atlantic helps address these knowledge gaps.

In this paper, we investigate the variability of biogeochemical properties (dissolved inorganic nutrients, dissolved inorganic carbon and total alkalinity) in the eastern subpolar North Atlantic and their transport in a branch of the upper limb of the AMOC. Specifically, we examine flows through the Rockall Trough, the easternmost basin of the subpolar North Atlantic which contains a branch of the North Atlantic Current and the European Slope Current [*Houpert et al.*, 2020]. Water carried in these currents exchange with the Northwest European Shelf [e.g. *Huthnance et al.*, 2022] as well as flowing northward over the Greenland-Scotland Ridge and into the Nordic Seas and Arctic [e.g. *Hansen and Østerhus*, 2000]. We use observations from the easternmost portion of the OSNAP mooring array (termed The Ellett Array), including data from moored biogeochemical sensors (dissolved oxygen and pH) along with analysis of discrete samples collected by a moored water sampler (dissolved inorganic nutrients and total alkalinity). To fully assess biogeochemical transports, including any long-term trends, it is important to understand high-frequency variability in both the volume transport and biogeochemical properties. While the seasonal variability of the volume transport has been reported [*Fraser et al.*, 2022; *Houpert et al.*, 2020], high-frequency variability in biogeochemical properties in the eastern subpolar North Atlantic are unknown. We therefore first discuss observed intra-annual variability before deriving biogeochemical properties throughout the water column using the approach of Brown *et al.* [2021]. By combining these observed and derived timeseries with volume transport estimates from the OSNAP project [*Fraser et al.*, 2022; *Houpert et al.*, 2020], we are able to examine the nutrient and carbon transports at 12-hourly timesteps, across all seasons, and over a three year time period. We extend this timeseries back to the start of the OSNAP array in 2014 (i.e. before the addition of the biogeochemical sensors) by using the same multiple linear regression method but applying it to temperature, salinity and pressure data only.

With the exception of Brown *et al.* [2021] who examined anthropogenic carbon transport using data from the RAPID mooring array at 26 °N in the Atlantic, previous estimates of biogeochemical transports come from hydrographic sections. Whilst these are valuable, they must be considered snapshots [e.g. *Brown et al.*, 2021; *Williams et al.*, 2011]. This is especially true in light of the highly variable velocity field associated with the AMOC [*Lozier et al.*, 2019] and its components [e.g. *Fraser et al.*, 2022; *Koman et al.*, 2022], and the fact that velocity is often the dominant control on biogeochemical transports particularly at intradecadal timescales [*Brown et al.*, 2021; *Robbins and Bryden*, 1994; *Zunino et al.*, 2015]. Additionally, there is a summer bias to the observations and therefore transport estimates at more northern latitudes due

to harsh winter sampling conditions. Yet, individual branches of the North Atlantic Current [*Houpert et al.*, 2020; *Houpert et al.*, 2018], the European Slope Current [*Fraser et al.*, 2022] and biogeochemical concentrations [e.g. *Hartman et al.*, 2015] all exhibit seasonality. By using continuous data from the OSNAP mooring array, we provide the first multi-annual year-round estimates of nutrient and carbon transports in the important eastern subpolar North Atlantic.

2 Data

We use data from The Ellett Array at approximately 57 °N in the Rockall Trough (Figure 1) which comprises of a mooring array and annual-biannual hydrographic sections.

2.1 Mooring data

The Ellett Array has two full-depth moorings (seabed to 50 m below the sea surface) in the eastern and western boundaries of the Rockall Trough (EB1 and WB1 respectively), and one short mooring in the western basin (WB2) (Figure 1). Originally, the array also had a bottom-mounted Acoustic Doppler Current Profiler mooring (ADCP1) to monitor the European Slope Current, but due to heavy losses related to bottom trawling, only a single 8-month record exists. Instead, we use reanalysis data bias-corrected to the observed 8-month mean to create a virtual ADCP1 record [*Fraser et al.*, 2022; *Houpert et al.*, 2020].

The moorings were first deployed in 2014 with Conductivity-Temperature-Depth (CTD) instruments and current meters. In 2017, biogeochemical sensors (dissolved oxygen (DO) and pH) were added. As vertical variability in the basin is greater than horizontal variability, these were deployed on a single mooring, EB1 (57.1 °N, 9.6 °W), located within the northward flowing Atlantic Water. In 2017-2018, a combined CTD-DO-pH instrument (SBE Deep SeapHOx) was deployed at 63 m and three combined CTD-DO instruments (SBE 37-SMP-ODO) at 750 m, 960 m and 1600 m. These depths monitor the surface mixed layer, and the upper reaches and center of the mid-depth oxygen minimum (Figure 1) which are parts of the water column where DO, nutrients and carbon are most likely to be influenced by non-conservative processes such as biological activity. In 2018-2020, the CTD-DO-pH instrument was again deployed at 63 m with a CTD-DO instrument at 750 m. An automated water sampler (McLane RAS) was deployed at 63 m during 2017-2018 with samples taken every 10 days throughout the 13-month deployment. These samples were poisoned with 0.02-0.05 % mercuric chloride *in-situ*. Upon recovery, samples were analyzed for dissolved inorganic nutrients (nitrite+nitrate – hereafter referred to as nitrate, phosphate, and silicate), dissolved inorganic carbon (DIC) and total alkalinity (TA). Analysis methods are given in the next section. Nitrate, silicate and TA values from the moored water sampler are similar to those collected from the lowered rosette during the hydrographic sections. This gives confidence that there are no contamination issues and that the mercuric chloride in the moored sampler was sufficient to prevent biological activity. DIC values from the moored sampler are significantly higher than the hydrographic section data (likely due to air ingress between recovery of the water sampler and removal of the samples) while phosphate values are also slightly elevated (unknown cause). These data are not discussed further.

The moored CTDs (including those combined with the DO and pH sensors) were calibrated using a pre-deployment and post-recovery calibration dip as described in Houpert *et al.* [2020]. However, the DO and pH sensors were calibrated *in-situ* to nearby post-deployment and pre-recovery calibration casts. The moored DO sensors were calibrated to the calibrated lowered DO sensor using the difference between two sensors in density space, while the moored pH sensors was calibrated to pH derived from water sample DIC and TA values using CO2SYS [*Sharp et al.*, 2020]. This *in-situ* calibration enables correction of a slow (days-months) pressure-related drift seen in DO that reverses upon bringing the instrument back to the surface [*Berx et al.*, 2019], although we only observed this drift in the instrument deployed at 1600 m. The pH sensor performed within the manufacture's specifications, with a deployment offset of 0.048 pH units and a drift of < 0.001 units per month. As we perform an in-field calibration similar to Johnson *et al.* [2017], the accuracy will be improved by an order of magnitude.

After calibration, all moored data were filtered with a 48-hour low-pass filter to remove tidal oscillations and interpolated onto a 12-hourly timestep as described in Houpert *et al.* [2020] and Fraser *et al.* [2022].

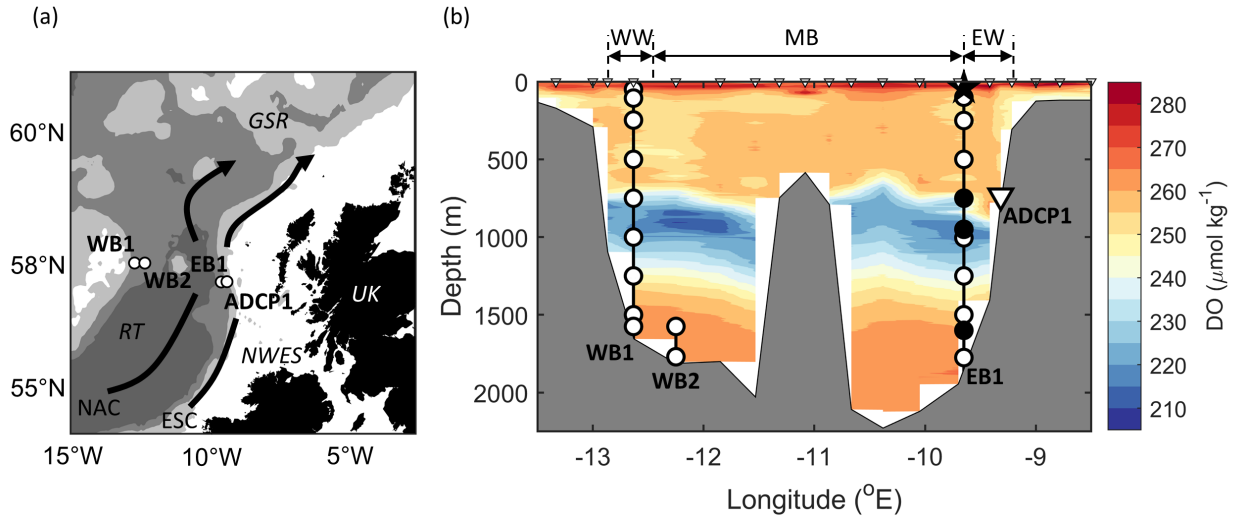

Figure 1. The Ellett Array. (a) Location of three moorings WB1, WB2 and EB1 and the virtual mooring ADCP1. Features labelled are the Northwest European Shelf (NWES), Green-Scotland Ridge (GSR), Rockall Trough (RT), European Slope Current (ESC) and North Atlantic Current (NAC). (b) Schematic of the Ellett Array in 2017-2018 superimposed on the July 2018 DO section. Moored CTD positions are shown as white circles, combined CTD and DO sensors by black circles, and the combined CTD, DO and pH sensor and moored water sampler by the black star. Also shown is the virtual mooring ADCP1 (white triangle), the standard hydrographic station positions (small white triangles) and the designations used in the volume transport calculation: Western Wedge (WW), Mid-Basin (MB) and Eastern Wedge (EW).

2.2 Hydrographic section data

Hydrographic sections across The Ellett Array were conducted in May 2017 (DY078), July 2018 (AR30-04) and October 2020 (DY120) using the historic Ellett Line station positions (Figure 1). In addition to lowered CTD and DO measurements, water samples were collected for sensor calibration and chemical analysis (Figure SM1). Samples to calibrate the lowered conductivity sensor were analyzed onboard using a Guildline Autosal and OSIL standard seawater. Samples to calibrate the lowered DO sensor were analyzed onboard following GO-SHIP protocols [*Langdon*, 2010] using a Metrohm 848 Titrino, internal standards and OSIL iodate standards. Samples for nitrate, phosphate and silicate were collected as per GO-SHIP protocols [*Becker et al.*, 2019] before being frozen and analyzed ashore using flow injection analysis (Lachat Quikchem 8500), certified reference materials (SCOR-JAMSTEC) and internal standards. Overall accuracies and precisions were 97 % and 2 % for nitrate, 98 % and 1 % for phosphate, and 96 % and 1 % for silicate. Samples for DIC and TA were collected and poisoned with 0.02 % mercuric chloride according to Dickson *et al.* [2007] before shore-based analysis using an Apollo SciTech AS-C3 DIC analyzer, and a Metrohm 848 Titrino Plus and Aquatrode electrode system respectively. Certified reference materials (Dickson) were used for the DIC and TA calibration and to assess accuracy. Typical accuracies and precisions were 0.1 % and ≤0.15 % for DIC, and 0.2 % and 1 % for TA.

Post-analysis, nutrient and carbon data were quality checked using procedures described in Tanhua *et al.* [2009]. Data were checked for intra-cruise consistency before a secondary inter-cruise consistency check was carried out using historical data from the Extended Ellett Line which had undergone its own quality procedure as described in Johnson *et al.* [2013]. No corrections were applied.

3 Methods

3.1. Derivation of nutrient and carbon below the surface

Below 63 m, nutrient and carbon observations were only made during the annual-biannual hydrographic sections. To obtain high-frequency records, we use predictive regression equations (PREs) as applied to moored data to investigate anthropogenic carbon transports by Brown *et al.* [2021]. Multiple linear regression based approaches have similarly been used to derive carbon parameters from hydrographic data [e.g. *Bostock et al.*, 2013; *Carter et al.*, 2016]. While neural network such as CANYON-B [*Bittig et al.*, 2018] can also be used, comparison of the two approaches show similar results with multiple linear regression having the advantage of simplicity and explicability [*Carter et al.*, 2021]. Our PREs describe each nutrient or carbon property in terms of potential temperature (θ), practical salinity (S_P), pressure (P), and where available DO (Equation 1). They are derived using the hydrographic section data and multiple linear regression, and are applied to the moored data to derive 12-hourly nutrient and carbon timeseries.

$$y = \beta_0 + \beta_1 \theta + \beta_2 S_P + \beta_3 P [+ \beta_4 DO] \quad (1)$$

where y is the predicted value (nitrate, phosphate, silicate, DIC or TA), β_0 the intercept, and β_{1-4} the regression terms. The multiple linear regressions were carried out using two predictor matrices: (1) θ, S_P, P and (2) θ, S_P, P, DO; enabling y to be predicted when moored DO data was, and was not, available. Each multiple linear regression was run twice, with the second iteration excluding outliers identified as values exceeding three times the mean Cooks Distance [*Brown et al.*, 2021]. The Root Mean Square Error (RMSE) and adjusted-R^2 values for the final linear models are given in Tables SM1-3.

When the predictor matrix included DO, the residuals (calculated by subtracting the predicted values for a hydrographic section from the measured values from the same section) showed no vertical structure. In the absence of DO, the residuals for each of the nutrients showed a pressure-bias (Figure SM2): predicted values were overestimated in the upper 200 m, underestimated between approximately 500-1250 m, and overestimated below around 1500 m. This is not dissimilar to the DO profile shape and likely reflects that biological processes are not captured fully when the predictor matrix excludes DO. To remove this vertical structure, we divided the water column into two regions: (1) depths above and below the mid-depth oxygen minimum, and (2) those within it, and created PREs for each. This separates data collected in parts of the water column where physical processes dominate and those in the oxygen minimum where biological processes play a larger role, with this step only done when the predictor matrix did not include DO. Although this approach successfully removes the vertical structure (Figure SM2), the adjusted-R^2 values in the oxygen minimum region are reduced to around 0.7 (Tables SM1-3). We did not subdivide our region horizontally (unlike Brown *et al.* [2021]) due to the small geographic extent. For TA, we found that excluding the surface mixed layer, defined here as the upper 50 m, greatly improved the linear model fit. However, the adjusted-R^2 values for this property (~0.65) are lower than for the other variables.

Rather than combining the data from each hydrographic section to create a single PRE per depth range and property (as done in Brown *et al.* [2021]), we create PREs for each hydrographic section and linearly vary the regression coefficients (β_{0-4}) temporally between these points. Advantages of this are that conditions at the time of each hydrographic cruise are represented, any temporal change in the relationship between the predictor variables and nutrients and carbon is captured, subsequent deployments can easily be added and no assumptions regarding growth rates for DIC need to be applied. Adjusted R^2 values and RMSEs are comparable to when PREs are derived using the data from the 2017, 2018 and 2020 hydrographic sections combined (Table SM4). The 2020 cruise was heavily impacted by COVID-19 restrictions: only three stations were occupied in the Rockall Trough with one tenth of the usual number of nutrient samples collected. To avoid errors due to this low sample number, the nutrient '2020' PREs were generated using the 2018 and 2020 data combined. For DIC and TA, the '2020' PREs were generated using the 2020 data only due to a temporal split between the 2018 and 2020 values and a reduced difference in sample numbers between the 2020 and previous cruises.

Comparison between the derived timeseries and measurements made within 50 m of the mean depth of the moored instrument (125 m for instruments deeper than 1500 m) during the annual-biannual hydrographic sections show the PREs perform well (Figure SM3-7). This applies both when DO is included in the predictor matrix and when it is not. DIC and TA exhibit slight trends

(below 1250 m for DIC and below the surface mixed layer for TA) but follow the discrete hydrographic data used in generating the relationships (Figure SM6-7).

3.2. Derivation of nutrient and carbon at the surface

During 2017-2018, water samples for nitrate, silicate and TA were taken at 63 m every 10 days by the autonomous moored sampler. To increase the frequency to 12-hourly timesteps (as for depths below 63 m) and create a record spanning 2017-2020, we again used PREs. This time they were derived using values from the moored water sampler in conjunction with θ, S_P, P and DO from the CTD-DO-pH instrument. This method accounts for any seasonality in the biogeochemical properties enabling surface values to be recreated more accurately (whereas the sub-surface PREs assume that the relationships derived apply year-round). The statistics for the surface PREs are summarised in Table SM5. As there are no usable phosphate or DIC data from the moored water sampler, both were determined in different ways. DIC was calculated from the surface derived TA timeseries and observed pH record from the CTD-DO-pH instrument using the CO2SYS software [*Sharp et al.*, 2020], this has the advantage of using one direct measurement from the surface layer. Phosphate was derived from the nitrate record using the mean nitrate:phosphate ratio from the 2017, 2018 and 2020 hydrographic sections.

We applied the above to all mooring records shallower than 90 m. To account for winter deepening of the surface mixed layer, we use moored temperature records to assess which instruments are in the mixed layer. For each timestep j between November and April, if the difference in temperature between depth i and 63 m ($\Delta T_{i\text{-}63,j}$) is ≤ 0.5 ˚C (T_{lim}), we use Equation 2 to apply a weighted surface-PRE derived value to the instrument at depth i ($BGCnew_{i,j}$):

$$BGCnew_{i,j} = (\Delta T_{i\text{-}63,j} * BGC_{i,j}) / T_{lim} + (1 - (\Delta T_{i\text{-}63,j} / T_{lim})) * BGC_{63,j} \quad (2)$$

where $BGC_{i,j}$ is the original biogeochemical value at depth i derived using the sub-surface PRE, and $BGC_{63,j}$ the biogeochemical value at 63 m derived using the surface PRE. We use this weighted approach to avoid abrupt transitions in the biogeochemical record at depth i as values move between those derived from the sub-surface and surface PREs. This application of the surface PRE to additional depths during November to April captures the deep homogeneous mixed layer during winter better than using the sub-surface PREs alone.

As the surface PRE created a few slightly negative (< 1 μmol kg^{-1}) silicate concentrations at the end of the summer, we created a constraint that concentrations could not be < 0 μmol kg^{-1}.

3.3. Calculation of biogeochemical transports

Nutrient and carbon fields were gridded on to a regular 20 dbar vertical grid to match the velocity field with the shallowest measured value (at 63 m during 2017-2020) extended to the surface. Biogeochemical transports were then calculated by combining the gridded nutrient and carbon fields with the velocity estimates from OSNAP. The methodology used to calculate the volume transport is fully described in Houpert *et al.* [2020] and Fraser *et al.* [2022] and combines transport estimates from the western wedge, mid-basin, and eastern wedge of the Rockall Trough (Figure 1). Transport in the western wedge, defined as 12.9 °W to the mid-point between moorings WB1 and WB2, is estimated from current meters on WB1. Transport in the

mid-basin, defined as the eastern boundary of the western wedge to mooring EB1, is calculated using moored hydrographic data and the thermal wind equation referenced to zero velocity at 1760 m. Transport in the eastern wedge, defined as the region between EB1 and 9.2 °W, is computed using current meters on EB1 and, due to the lack of sustained observational data in the European Slope Current, output from the GLORYS12V1 reanalysis [*CMEMS*, 2022] bias-corrected to the single 8-month successful ADCP1 deployment. This 2014-2020 virtual ADCP1 record is used to calculate velocities in the eastern wedge east of ADCP1. For areas between ADCP1 and EB1, velocities above 750 m are linearly varied between the two records, whilst below 750 m only velocities from EB1 are used. As Ekman Transports in the Rockall Trough are small [2014-2018 mean 0.2 Sv, *Houpert et al.*, 2020], these are not included in the volume transport estimate.

We use the nutrient and carbon profiles derived at mooring EB1 to calculate biogeochemical transports (Q_C) across the width of the Rockall Trough (Equation 3).

$$\boldsymbol{Q_C = \int_{-H}^{0} CV dz} \quad (3)$$

where V is the volume transport perpendicular to the section per unit depth (i.e. the transport in the western wedge, mid-basin and eastern wedge combined), C the nutrient or carbon volumetric concentration profile, z the depth co-ordinates and H the water depth.

3.4 Uncertainty estimation

We consider three uncertainties for the biogeochemical transports: (1) those associated with the derivation of the nutrient and carbon fields, (2) those related to the computation of the velocity field, and (3) the combined or total transport uncertainty. As the nutrient and carbon transports are calculated by multiplying the chemical concentration by the volume transport (Equation 3), we use the standard formula for combining errors when using multiplication. We use the RMSE associated with the PREs for uncertainty (1), and the published RMSE associated with the volume transport estimate [0.92 Sv, *Houpert et al.*, 2020] for uncertainty (2). For the calculation of uncertainties (1) and (2), we held the RMSE associated with the other input at zero; whilst for the total uncertainty we used both the concentration and volume RMSEs as inputs. The resulting transport uncertainties (Table SM6) show that uncertainties (1) and (2) are similar in magnitude, with the total uncertainty being around one fifth that of the natural variability (defined as one standard deviation of the mean transport).

4 Results

To fully understand biogeochemical transports including any long-term trends, knowledge of the high-frequency variability of both the volume transport and biogeochemical properties is required. Whilst the seasonal signal of the volume transport through the Rockall Trough has been investigated [*Fraser et al.*, 2022; *Houpert et al.*, 2020], the intra-annual variability in carbon and nutrients in the region are yet to be quantified. Before discussing the biogeochemical transports, we therefore first describe the seasonal variability in the biogeochemical properties.

4.1. Seasonal variations in mixed layer depth

We start by examining the evolution of the surface mixed layer throughout the year to assess when moored instruments are representative of this layer. We use the conservative temperature timeseries from the five shallowest moored instruments on EB1 (63 m to 750 m, Figure 2.a) which cover the range of winter convection in the Rockall Trough. The mixed layer depth reaches around 106 m in early November each year (as evidenced by the records at 63 m and 106 m converging to the same value) and at least 252 m by December. The maximum convection depth varies interannually; in winter 2017/2018 the mixed layer reaches 500 m in March, in 2018/2019 the maximum mixed layer depth is less than 500 m, while during winter 2019/2020 the mixed layer extends to 500-750 m in February and March. Although the deepening of the mixed layer is gradual, restratification is more rapid with timeseries at multiple depths diverging near concurrently in April.

As the shallowest moored instrument is at 63 m, we use profiles from cruises between 2012-2020 to examine mixed layer depth above this level (Figure 2.b). For 2017-2020, we use The Ellett Array hydrographic sections, while for 2012-2016 we use data from the Extended Ellett Line. Each profile is from -9.700 °W, 57.152 °N which is within 10 km of EB1. The profiles were collected between mid-May to mid-October and thus cover the part of the year where we expect the shallowest surface mixed layer. Although there is interannual variability, the mixed layer is around 50 m in May, 20-25 m in June, 15-20 m in July and about 10 m in August. By October, mixed layer depth increases to around 60 m.

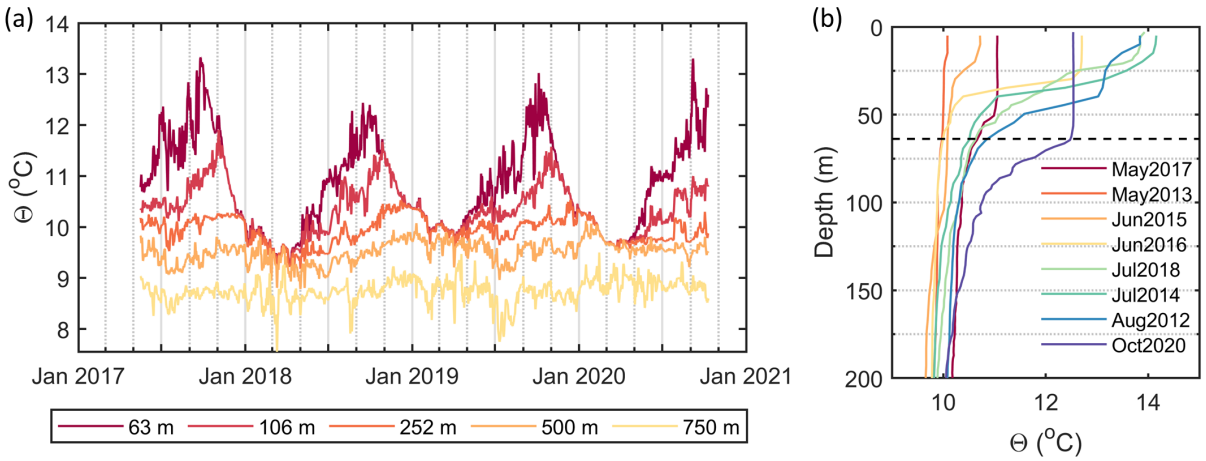

Figure 2. Evolution of the surface mixed layer at mooring EB1. (a) Conservative temperature timeseries from the top five moored CTD instruments on EB1. (b) Conservative temperature profiles within 10 km of the EB1 location measured during Extended Ellett Line (2012-2016) and Ellett Array (2018-2020) cruises. The dashed line shows the mean depth of the moored water sampler and combined CTD-DO-pH instrument on EB1.

4.2 Seasonal variability in observations at 63 m

The instruments at 63 m on mooring EB1 (CTD-DO-pH and automated water sampler) are within the surface mixed layer between approximately October to April, and immediately below this in the seasonal thermocline between roughly May to September (Figure 2.b). Temperature,

salinity, DO and pH records show reduced higher-frequency variability between October and April when the instrument is within the homogenous mixed layer, and increased variability between May and September when it is within stratified water (Figure 3.a).

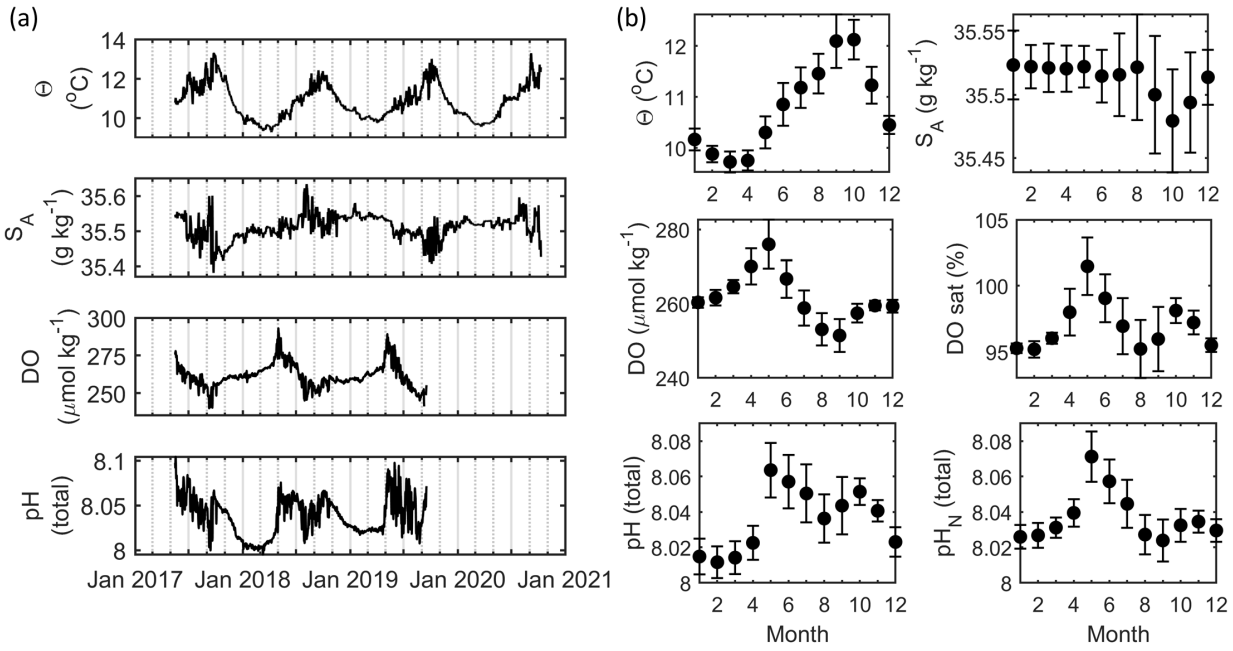

Figure 3. Data from the CTD-DO-pH instrument at 63 m on EB1. (a) Conservative temperature, absolute salinity, DO and pH against date. The DO and pH record ends in mid-September 2019 due to battery failure. (b) Monthly mean (circles) ± 1 standard deviation (error bars) of conservative temperature, absolute salinity, DO saturation, pH and temperature-normalized pH (pH_N).

Temperature, DO and pH show distinct seasonal variability although the signal for salinity is less clear (Figure 3.a). To examine these seasonal changes, we calculate monthly means and associated standard deviations (Figure 3.b). Temperature has a minimum in March/April and a maximum in September/October with a peak-peak amplitude of 2.4 °C and little interannual variability (i.e. the error bars in Figure 3.b mostly represent intra-monthly variations). Monthly mean salinity is near constant between December and August with no seasonal maximum. A minimum (35.48 ± 0.04 g kg^{-1}) is seen in October although variability between July and November is high due to large interannual differences. Monthly mean DO concentrations show a maximum in May (276 ± 6.6 µmol kg^{-1}) and a minimum in September (251 ± 4.4 µmol kg^{-1}) with the standard deviation largely due to intra-monthly variability. As water temperature and to a lesser extent salinity affects DO solubility, we calculate DO saturation. Like DO concentrations, monthly mean DO saturations show a maximum in May when levels are supersaturated (101 %). However, DO saturations show a secondary maximum in October (98 ± 1 %) and November, and minima in August and February (95 ± 1 %). The seasonal cycle of pH is similar to that of DO saturation with a maximum in May (8.06 ± 0.02), a smaller secondary maximum in October (8.05 ± 0.01), and a minimum in February (8.01 ± 0.01). We also consider pH normalized to a constant temperature (pH_N). To calculate pH_N we defined the relationship between temperature and pH using CO2SYS [*Sharp et al.*, 2020] as advised by Hu [2022], using the mean salinity, pressure, DIC, TA, silicate and phosphate levels at 63 m. This was then

applied to the pH record to create a record normalized to the mean temperature at 63 m (10.85 °C). The seasonal cycle of pH_N is similar to pH although the maximum in May is enhanced whilst the secondary maximum in October is more muted. DO saturation, pH and pH_N all show a marked increase between April and May (3.5 %, 0.04 and 0.03 respectively).

Nitrate and silicate records from the moored water sampler also show clear seasonal variability (red circles, Figure 4). Although there are only 13 months of observations, the novelty of these mean that we again calculate monthly means with associated standard deviations (Figure 4.b). Nitrate has a maximum in February (10.7 ± 0.3 µmol kg^{-1}) and a minimum in October (4.7 ± 0.6 µmol kg^{-1}). Concentrations decline by -2.4 µmol kg^{-1} between April and May before a steady decline to the minimum in October. Silicate has a maximum in April (4.4 ± 0.3 µmol kg^{-1}) with a pronounced decline of -2.3 µmol kg^{-1} between April and May. Concentrations then remain relatively constant throughout the rest of the summer until levels start to increase in November. Monthly means created using the 28 months of data from the surface PREs (not shown) have similar patterns of variability with contemporaneous minima and maxima. Neither nitrate or silicate data from the moored water sampler or hydrographic sections reach 0 µmol kg^{-1}, although concentrations less than 1.0 µmol kg^{-1} were observed in May-June 2017 and June 2018.

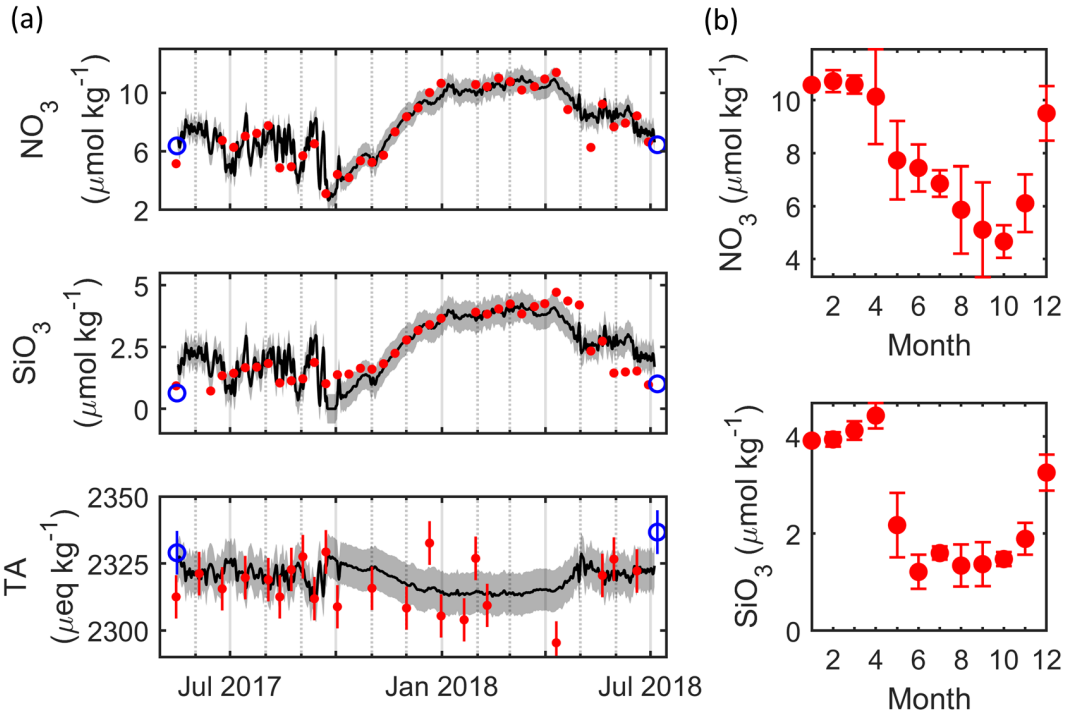

Figure 4. Data from the moored water sampler at 63 m on EB1. (a) Nitrate, silicate and TA against date. (b) Monthly mean concentrations (circles) ± 1 standard deviation (error bars) of nitrate and silicate. Red filled circles show observations from the moored water sampler, blue circles data from the hydrographic sections and the black line the surface PREs derived values with ± 1 RMSE associated with the PRE (Table SM5). For (a) vertical lines show the analytical precision of the samples (section 2.2), for the nutrients these are too small to be visible.

4.3 Dissolved oxygen observations

In addition to the instrument at 63 m, DO sensors were deployed at 750 m, 960 m and 1600 m during 2017-2018, and 750 m in 2018-2020 (Figure 5). Although there are some mooring knockdowns by strong currents, these are fairly small; the largest knockdown at the top of the mooring is 93 m although most events are less than 40 m, while knockdowns at 1600 m are smaller than 2 m. Mean DO concentrations are highest at 63 m and 1600 m (~260 ± 8 µmol kg^{-1}), and lowest at 960 m (218 ± 4 µmol kg^{-1}). When DO saturations are considered, higher levels are seen at 63 m than 1600 m (97 ± 3 % compared to 83 ± 0.3 %), whilst the lowest values are again seen at 960 m (75 ± 1.3 %). Only the instrument at 63 m shows a clear seasonal signal, as expected from the deployment depths relative to observed winter convection depth (Figure 2). The largest variability in DO is observed at 750 m rather than 63 m (± 11 µmol kg^{-1} compared to ± 8 µmol kg^{-1} at 63 m). This instrument is located in a strong vertical gradient of DO (Figure 5.b) as concentrations move from well-oxygenated Atlantic Waters to lower levels within the mid-depth oxygen minimum layer. The smallest variability is at 1600 m (± 0.6 µmol kg^{-1}) which is close to instrumental precision and less than the pressure-related drift removed during processing.

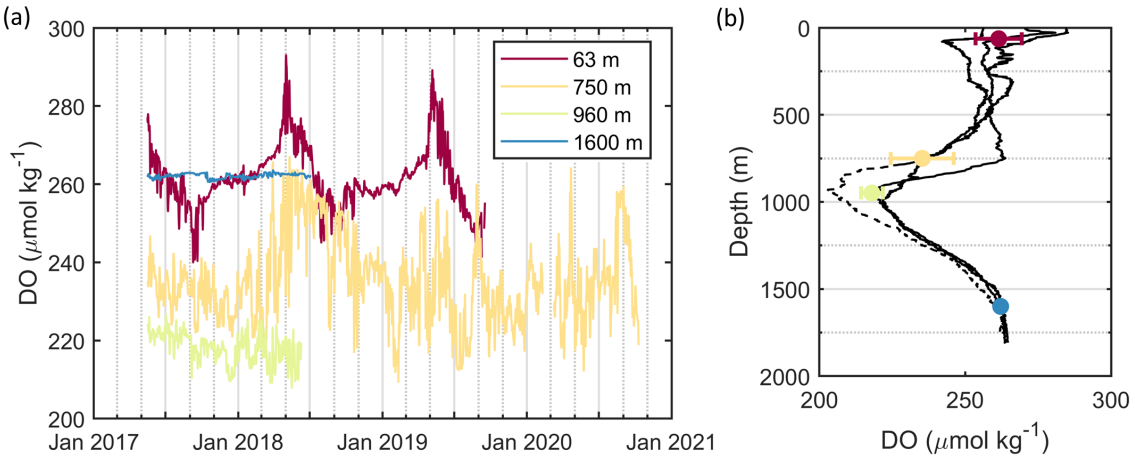

Figure 5. Observed DO concentrations at different depths on mooring EB1. The record from 63 m shown on Figure 3.a is duplicated here. Filled circles on (b) show the mean DO concentration and the errors bars ± 1 standard deviation. Black lines are lowered DO profiles from the station closest to EB1 in May 2017, July 2018 and October 2020 with the 2020 profile being dashed below 800 m due to moored timeseries below this covering the period 2017-2018 only.

4.4 Derived nutrients and carbon fields

The nutrient timeseries derived from the two shallowest instruments on EB1 (63 m, 106 m) exhibit a clear seasonal signal, with maxima in March and minima in October at 63 m and a month later in November at 106 m (Figures SM8-10). At 252 m, the seasonal cycle is shifted with maxima in March-May, and minima between November and January. This shift is more pronounced at 500 m with maxima in July and minima in December-March. The peak-peak magnitude of the seasonal cycle decreases with depth; for example for silicate this is 2.6 µmol kg^{-1} at 63 m, 1.7 µmol kg^{-1} at 107 m, and 0.6 µmol kg^{-1} at 252 m and 500 m. These deeper

seasonal cycles are within errors associated with the PREs (Tables SM1-3,5) and standard deviation error bars around the monthly means (Figures SM8-10).

Nitrate and phosphate have a mid-depth maximum associated with the minimum oxygen layer with concentrations of 17.8 ± 0.6 μmol kg^{-1} and 1.2 ± 0.04 μmol kg^{-1} respectively (Figure SM3-4). Silicate does not show a mid-depth maximum, although concentrations at 1000 m (9.4 ± 0.5 μmol kg^{-1}) are elevated (Figure SM5). DIC has a mid-depth maximum (2171 ± 5 μmol kg^{-1}, Figure SM6) whilst little vertical structure is observed for TA (Figure SM7) with variability through the water column being 19 μeq kg^{-1}. The largest variability for nitrate, phosphate and silicate is seen at 63 m with very little variability observed below the mid-depth oxygen minimum. This is true even when DO was measured at 1600 m in 2017-2018 and included in the predictor matrix.

4.5 Nutrient and carbon transports

Mean nutrient and carbon transports for 2017-2020 are northwards (Table 1) although flow is highly variable (Figure 6.a). Southward transports are observed, mostly for 48 hours or less, although a 33-day period of southward flow occurred between 29th June 2017 and 31 July 2017. Partial correlation coefficients between the volume transport and each biogeochemical transport, when accounting for temporal changes in the chemical property, exceed 0.98 with all being statistically significant at the 99 % level. Thus, for 2017-2020, variability in the volume transport, rather than changes in the carbon or nutrient fields, dominates the biogeochemical transport variability. This is emphasized in Figure 6.b which compares the silicate transport resulting from temporally-varying volume transport profiles and a time-mean silicate profile, against that calculated using a time-mean volume transport profile and time-varying silicate profiles. Although we only show the silicate transport here (Figure 6a-b), the other nutrient and carbon transport timeseries look identical in terms of variability with only the transport values changing between properties.

	May 2017 – Oct 2020 ***θ, S_P, P, DO***	***May 2017 – Oct 2020*** ***θ, S_P, P***	***Jul 2014-Oct 2020*** ***θ, S_P, P (2014-2017)*** ***θ, S_P, P, DO (2017-2020)***
Q_{VOL} (Sv)	4.53 ± 3.44 -	4.53 ± 3.44 -	4.86 ± 3.34 -
Q_{NO3} (kmol s^{-1})	51.36 ± 44.04 (11.3)	50.76 ± 43.47 (11.2)	56.17 ± 43.80 (11.6)
Q_{PO4} (kmol s^{-1})	3.42 ± 2.92 (0.8)	3.39 ± 2.89 (0.7)	3.76 ± 2.91 (0.8)
Q_{SiO3} (kmol s^{-1})	19.97 ± 19.71 (4.4)	19.22 ± 19.08 (4.2)	22.12 ± 19.89 (4.6)
Q_{DIC} (kmol s^{-1})	9318 ± 7098 (2058)	9323 ± 7104 (2059)	10,357 ± 7161 (2130)
Q_{TA} (keq s^{-1})	10,070 ± 8174 (2364)	10,706 ± 8176 (2364)	11,522 ± 7953 (2370)

Table 1. Nutrient (nitrate, phosphate and silicate) and carbon (DIC, TA) transports through the Rockall Trough for different time periods and predictor matrices. For each transport, the mean and standard deviation is given, along with the transport-weighted property (brackets). This is defined as the biogeochemical transport divided by the volume transport and has units of mmol m^{-3} or meq m^{-3} for TA. Positive transports are northward.

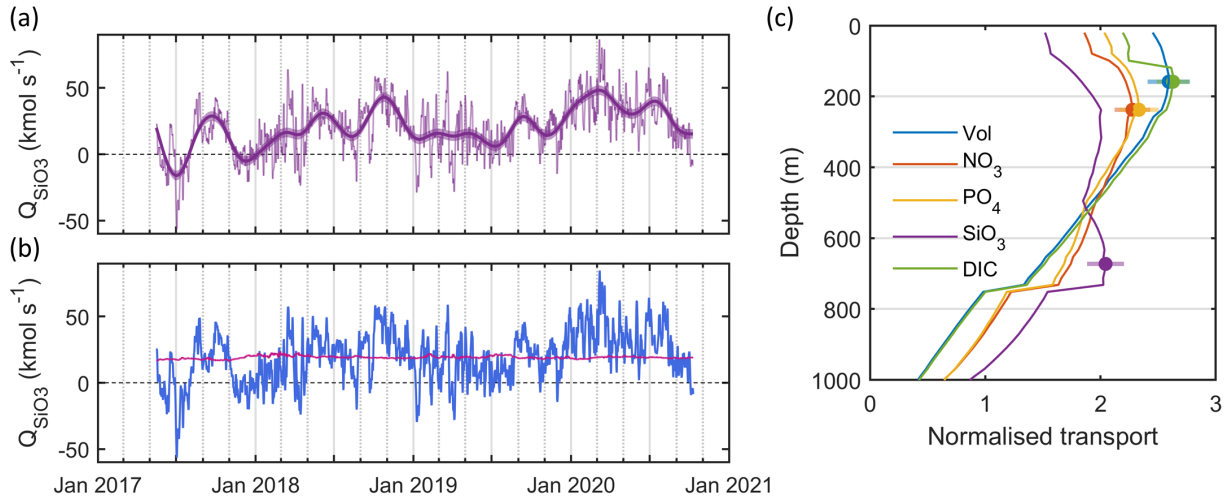

Figure 6. (a) Transport of silicate through the Rockall Trough, (b) decomposed into that resulting from variations in the volume transport (blue) and silicate concentrations (pink). This was calculated using time-varying volume transport profiles and a time-mean silicate profile, and a time-mean volume transport with time-varying silicate profiles respectively. In (a) and (b), the thin line shows the 12-hourly timeseries, while the thick line in (a) shows a 90-day low pass filtered timeseries and the shading envelope ± 1 error (Table SM6). (c) normalized transport per 20 m depth bin over the upper 1000 m for volume (blue), nitrate (orange), phosphate (yellow), silicate (purple) and DIC (green). TA is not shown as it is identical to DIC.). Filled circles show the depth of the maximum transport for each property and the horizontal line the associated transport error (Table SM6). Positive transports are northward.

The maximum volume transport is observed at 160 m with this then decreasing over the upper 1000 m (blue, Figure 6.c). The biogeochemical transport profiles are defined by the interplay between the velocity and chemical profiles. DIC and TA transport profiles (green, Figure 6.b) are similar to that for volume, although transports in the upper 120 m are reduced due to the lower concentrations in this part of the water column. Nitrate and phosphate have a deeper maximum transport at 240 m and a broader less-pronounced peak. Silicate has a broad peak of transports between 120 m and at least 730 m with two maxima in transports at 315 m and 675 m.

As variability in the 2017-2020 biogeochemical transports are dominated by volume transport variability, we extend the biogeochemical transports back to the start of The Ellett Array measurements in 2014. We do this by using the PREs generated in 2017 (Table SM1) with a predictor matrix of θ, S_P, P only. The 2017-2020 mean transports calculated both including and excluding DO are near identical in magnitude, with only DIC having a larger difference of 6 % (Table 1). This suggests that the lack of DO measurements before 2017 will not significantly affect the mean transport, though the uncertainties will be slightly larger due to higher RMSE and lower adjusted-R^2 values associated with the PREs when DO is not included (Table SM1). The use of the 2017 PREs with the moored data creates time-varying nutrient and carbon fields, however, it assumes that the relationships derived in 2017 apply for the 2014-2017 period. Prior to 2017, the shallowest measurement on EB1 was at 83 m rather than 63 m. We apply the surface PRE to this instrument and follow the method detailed in section 3.

The six-year mean transports through the Rockall Trough are again northwards and highly variable (Table 1). Mean transports are lower for 2017-2020 than for 2014-2020 for all properties with the variability similarly reduced. For the nutrients and TA, this is almost entirely explained by the lower volume transports during 2017-2020 as evidenced by the near identical transport weighted property values between the two periods (brackets, Table 1). The transport weighted property for DIC is 3 % higher for 2014-2020 than 2017-2020, this is due to changes in the mid-water column between 2014-2020 although this is likely within errors.

5 Discussion

Data from the moored CTD-DO-pH instrument and automated water sampler at 63 m show clear intra-annual variability related to both physical and biological processes. DO concentrations/saturations and pH increase between April and May while nitrate and silicate concentrations decrease. These changes are likely due to the spring bloom that acts to deplete nutrient concentrations, increase DO levels due to photosynthesis, and reduce carbon dioxide levels, which due to carbonate chemistry, leads to an increase in pH. The large decrease in silicate (from 4.4 μmol kg^{-1} in April to 2.1 μmol kg^{-1} in May) suggests that the early bloom is dominated by diatoms as found by other studies [e.g. *Daniels et al.*, 2015; *Henson et al.*, 2012]. DO saturation and pH have a secondary peak in October. This may be due to an autumn bloom which are known to occur in the North Atlantic [e.g. *Binetti et al.*, 2020; *Martinez et al.*, 2011] although as the peak in pH_N is more muted, some of the pH signal is likely related to temperature changes. Nitrate concentrations decrease throughout the summer to a minimum in October, while silicate values remain near constant between June and October at < 2 μmol kg^{-1}. This suggests that phytoplankton requiring nitrate, rather than silicate, dominate after the initial spring bloom

and during the autumn bloom. The autumn bloom may also be fueled by intermittent nutrient input into the surface mixed layer driven by storms [as observed in the Porcupine Abyssal Plain, *Binetti et al.*, 2020] which is not captured by the moored water sampler. Seasonal cycles are largest at the surface and decrease with depth. While the moored instruments and associated derived timeseries at 500 m show a small seasonal cycle, this is absent at 750 m, probably due to the surface mixed layer not extending to this depth during 2017-2020. The largest variability in DO is observed at 750 m rather than at 63 m. This is due to the 750 m instrument being in a strong vertical gradient of DO as concentrations move between the well-oxygenated Atlantic waters and the oxygen minimum layer with the variability likely to result from isopycnal heave.

The mean biogeochemical transports through the Rockall Trough are northwards and highly variable due to changes in the volume transport. Periods of southward flow occur, with the longest of these being 33 days in 2017. This re-enforces the need to treat transport estimates from hydrographic sections as snapshots as highlighted by Williams *et al.* [2011] and Brown *et al.* [2021]. It also infers large uncertainties on nutrient and carbon budgets estimated using two hydrographic sections separated by latitude and time. Although the use of mean transport estimates from multiple hydrographic sections ameliorates this, this approach can only derive a decadal signal. Thus, there are advantages in using estimates from mooring arrays; particularly relating to the provision of high frequency timeseries and the removal of seasonal bias in the transport estimates related to seasonality in the volume transport [e.g. *Fraser et al.*, 2022; *Houpert et al.*, 2020; *Houpert et al.*, 2018] or biogeochemical properties [this paper, *Hartman et al.*, 2015].

As observed in the Gulf Stream [*Pelegrí and Csanady*, 1991; *Williams et al.*, 2011], the maximum nutrient transports in the eastern subpolar North Atlantic are deeper in the water column than the maximum in the velocity transport. Additionally, the depth of maximum transport varies by biogeochemical property. Nitrate and phosphate both have a maximum transport at 240 m, whilst silicate transport has two maxima at 315 m and 675 m and a broader less pronounced peak. In contrast, the maximum DIC and TA transports are at the same depth (160 m) as the maximum velocity transport.

During 2017-2020, variability in the volume transport, rather than in the carbon or nutrient concentrations, dominated the biogeochemical transports variability. However, this may not be true on longer timescales due to sub-decadal to decadal variations in the biogeochemical fields. Atlantic Water nutrient concentrations vary on multi-annual timescales due to variations in the relative proportions of nutrient-poor water masses from south of the basin versus nutrient-rich subpolar water masses as the subpolar gyre changes strength. In the Rockall Trough, variations in the extent of the subpolar gyre and the related water mass redistribution affect nitrate and phosphate concentrations [*C. Johnson et al.*, 2013], with changes in silicate observed further west [*Hátún et al.*, 2017]. When subpolar water masses dominate the Rockall Trough, such as in 1996, nitrate and phosphate concentrations integrated between 200-700 m and averaged over the width of the basin are 12.44 μmol kg^{-1} and 0.81 μmol kg^{-1} respectively. When southern-origin water masses dominate, such as in 2008, nitrate and phosphate concentrations over the same depth range are lower at 10.31 μmol kg^{-1} and 0.66 μmol kg^{-1} respectively [*C. Johnson et al.*, 2013]. Between 2017-2020, the mean concentrations calculated using the same methodology as Johnson *et al.* [2013] were 12.1 ± 0.4 μmol kg^{-1} and 0.80 ± 0.02 μmol kg^{-1} for nitrate and phosphate respectively. Thus, the nutrient transports during our measurement period are more

akin to the mid-1990s when nutrient-rich subpolar water masses were more prevalent. To evaluate nitrate and phosphate transports during times when nutrient-poor subtropical or intergyre water masses dominate, we recalculate the 2017-2020 transports using the nutrient profiles collected at the Ellett Line station closest to mooring EB1 during 2008 (i.e. a time-constant nutrient profile). We corrected the upper 500 m of the nitrate and phosphate profiles for the respective seasonal signal using monthly averages of the derived variables from the top four moored instruments on EB1 (63 m, 106 m, 252 m, 500 m). We linearly interpolated these seasonal corrections between moored instrument depths and extended the correction at 63 m to the surface. If the volume transport remains constant, during a weak subpolar gyre when nutrient-poor water masses from south of the basin dominate, transports through the basin are 15 % lower for nitrate and 19 % lower for phosphate (Table 2). These differences are statistically significant at the 99 % confidence level. The ratio of nitrate to phosphate transport changes slightly between the two regimes, from 15.1:1 kmol s^{-1} during a strong subpolar gyre to 15.6:1 kmol s^{-1} when the gyre is weaker.

	Transport strong subpolar gyre	**Transport weak subpolar gyre**
Q_{NO3} (kmol s^{-1})	51.36 ± 44.04 (11.3)	44.36 ± 38.37 (9.8)
Q_{PO4} (kmol s^{-1})	3.42 ± 2.92 (0.8)	2.83 ± 2.46 (0.6)

Table 2. Effect of changing nitrate and phosphate concentrations on their transport through the Rockall Trough assuming a non-varying volume transport. For the strong subpolar gyre, transports measured during 2017-2020 are used (i.e. Table 1). For the weak subpolar gyre, transports are estimated using nutrient profiles collected in 1996 multiplied by the 2017-2020 volume transport. Transports are mean ± 1 standard deviation. The transport-weighted property (brackets) is defined as the biogeochemical transport divided by the volume transport and has units of mmol m^{-3} or meq m^{-3} for TA. Positive transports are northward.

Model studies suggest that volume transport at the southern entrance to the Rockall Trough varies with the strength of the subpolar gyre, with greater northward transports when the subpolar gyre is more energetic [*Hátún et al.*, 2005]. Observations also suggest a higher volume transport in the early 1990s (i.e. a stronger subpolar gyre) compared to the late 1990s (i.e. a weaker subpolar gyre) [*Bersch*, 2002], although as the velocity field is highly variable, aliasing must be considered. Model evidence additionally suggests that the European Slope Current is less strong when the subpolar gyre is weaker [*Marsh et al.*, 2017]; between 1988-1997 and 1998-2007, volume transport at The Ellett Array latitude decreased by -2.3 Sv (~45 % reduction). These concurrent reductions in volume transport will act to amplify the effect of the lower concentrations on nitrate and phosphate transports.

Water flowing northward through the Rockall Trough exchanges with the Northwest European Shelf and feeds into the northern North Sea [*Huthnance et al.*, 2022]. Model estimates of the Fair Isle Current which transports oceanic water into the North Sea, shows a reduction of ~7 % between 1988-1997 and 1998-2007 [*Marsh et al.*, 2017]. The combined effect of a reduction in

the Atlantic Water inflow into the North Sea during a weak subpolar gyre, coupled with a lower transport weighted property (Table 2), could lead to nitrate and phosphate transports being 22 % and 26 % lower relative to a strong subpolar gyre. In contrast, silicate transports may only decrease by around 7 % due to the absence of concentration changes in the Rockall Trough [*Hátún et al.*, 2017; *C. Johnson et al.*, 2013]. It is uncertain if ocean-shelf exchange elsewhere would change in response to a weakening gyre, although there may be contemporaneous changes in large-scale atmospheric circulation patterns and storm tracks which partly drive cross-shelf exchange. As nitrate and phosphate transport weighted concentrations decrease (Table 2), nitrate and phosphate transports onto the shelf would decrease by 15 % and 19 % respectively even if the volume exchange remained constant. Any net change in nutrients on the Northwest European Shelf is dependent on multiple factors including the balance between transport weighted concentrations on and off the shelf [*Huthnance et al.*, 2022] and changes in local cross-shelf transport mechanisms [*Jones et al.*, 2020; *Pätsch et al.*, 2020]. However, the ocean is an important source of nutrients to the Northwest European Shelf [*Proctor et al.*, 1993], with changes in the on-shelf supply affecting primary productivity [*Holt et al.*, 2012], carbon sequestration [*Chaichana et al.*, 2019; *Humphreys et al.*, 2019] and shelf ecosystems [*Heath and Beare*, 2008]. Thus, we speculate that changes in the subpolar gyre may drive multiple changes on the Northwest European Shelf.

The Atlantic Water flowing through the Rockall Trough is also an important source of nutrients to the Arctic [*Torres-Valdés et al.*, 2013], particularly to the Barents Sea where it supports high primary productivity and carbon uptake [*Juranek*, 2022]. Nutrient concentrations within the Atlantic Water have declined over the past three decades. In the Eurasian Arctic, nitrate and phosphate concentrations at 200-300 m decreased at a rate of -0.4 μM decade^{-1} and -0.06 μM decade^{-1} respectively between the start of the record in 1994 and end of the record in 2018 [*Tuerena et al.*, 2022]. Faster declines were observed at shallower depths. A non-independent nitrate dataset from the Barents Sea Opening shows a decrease in nitrate between 0-200 m from 1984 to 2010 at a rate of -0.7 μM decade^{-1} [*Oziel et al.*, 2017]. In the western Nordic Seas, declines in silicate, at a rate of -0.7 μM decade^{-1}, have been observed at multiple sections from 1990 to 2015 with a contemporaneous increase in salinity and smaller decline in nitrate [*Hátún et al.*, 2017; *Rey*, 2012]. Upstream in the eastern subpolar North Atlantic, declines in nitrate and phosphate in the Rockall Trough were at a faster rate of -2 μM decade^{-1} and -0.12 μM decade^{-1} between 1996 and 2012 [*C. Johnson et al.*, 2013]. Again, concurrent increases in temperature and salinity were observed. Declines in silicate, at a rate of around -0.7 μM decade^{-1} between 1990 and 2015, were observed further west in the Iceland Basin, Irminger Basin and Faroese Shelf, as well as an advected signal in the boundary of the Labrador Sea [*Hátún et al.*, 2017].

As the subpolar gyre weakens and contracts, increases in temperature and salinity in the eastern subpolar North Atlantic propagate northward through the western Nordic Seas and into the Barents Sea [*Holliday et al.*, 2008]. Similar to Rey [2012], Tuerena *et al.* [2022] and Fransner *et al.* [2023], we suggest that part of the decreasing nutrient signal in the Barents Sea and wider Eurasian Arctic is an advective signal originating in the eastern subpolar North Atlantic. It is hypothesized that these nutrient reductions may limit Arctic primary productivity, with subsequent effects on ecosystems, fisheries and food security of Arctic nations [*Rey*, 2012; *Tuerena et al.*, 2022]. Thus, understanding nutrient transports in the eastern subpolar North Atlantic may improve our ability to predict future impacts upstream in the Arctic. A recent study has shown that advected nitrate anomalies from the subpolar North Atlantic enable the

abundance of phytoplankton in southern ice-free parts of the Barents Sea to be predicted up to five years in advance. In contrast, sea-ice appears to be a more important driver further north in the polar domain [*Fransner et al.*, 2023]. In 2016, salinities within the Atlantic Water in the eastern subpolar North Atlantic decreased to a level not seen in at least 120 years [*Holliday et al.*, 2020] due to increased freshwater from the Labrador Sea entering eastern regions [*Fox et al.*, 2022; *Holliday et al.*, 2020; *Jutras et al.*, 2023]. We speculate that a contemporaneous change in nutrients may also have occurred. Nitrate and phosphate concentrations in the Rockall Trough during 2017-2020 were comparable to those during 1996 when the subpolar gyre was relatively strong. The freshening reached the western Barents Sea in approximately 2018 [*Gonzalez-Pola et al.*, 2022]. If processes in the eastern subpolar North Atlantic play an important role in determining nutrient concentrations in the Eurasian Arctic, the observed decline in the region may start to slow or reverse.

6 Conclusions

In this paper we have examined high-frequency changes in nutrients and carbon in the eastern subpolar North Atlantic between 2017-2020. Novel measurements from an automated water sampler and moored biogeochemical sensors reveal increases in surface pH and DO and contemporaneous decreases in silicate and nitrate associated with a spring and autumn bloom. We apply PREs derived from hydrographic section data to high-frequency moored data to derive carbon and nutrient transports through the eastern subpolar North Atlantic for the first time. Transports for each biogeochemical property are northwards and highly variable with periods of southward flow. This reinforces the need to treat transports and budgets estimated from hydrographic sections as snapshots. Comparison with historical data suggests that nutrient concentrations in the upper waters of the eastern subpolar North Atlantic between 2017-2020 were comparatively high and indicative of a more energetic state of the subpolar gyre. Reducing nitrate and phosphate concentrations during a weak subpolar gyre can lower the nitrate and phosphate transports through the basin by 15 % and 19 % respectively. These changes may be amplified by contemporaneous reductions in volume transport; in particular, nitrate and phosphate transport into the northern North Sea may reduce by 22 % and 26 % respectively. In contrast, silicate transport will reduce by only around 7 % due to the absence of concentration changes. Thus, the ratio of the different nutrients transported onto the shelf may vary temporally. We speculate that the reduction in nutrient transport onto the shelf may produce changes in on-shelf primary productivity and carbon drawdown as well as pelagic ecosystems. In addition to being a source of nutrients to the Northwest European Shelf, the eastern subpolar North Atlantic is a source of nutrients to the Eurasian Arctic. Declines in nutrient concentrations have been observed along the advection pathway from the eastern subpolar North Atlantic, to the western Nordic Seas and into the Barents Sea. In the same way that temperature and salinity signals are propagated northward, we suggest that at least part of the nutrient decline in the Eurasian Arctic is explained by advection with the signal originating in the eastern subpolar North Atlantic. We speculate that the recent freshening and nutrient increases observed in the eastern subpolar North Atlantic may become evident in the Arctic timeseries enabling the magnitude of the advective signal versus local processes to be determined.

Acknowledgments

This study has received funding from the European Union's Horizon 2020 Research and Innovation Programme under grant agreement nos. 678760 (ATLAS), 818123 (iAtlantic) and 633211 (AtlantOS). The output of this study reflects only the author's view, and the European Union cannot be held responsible for any use that may be made of the information contained therein. Support has also been received from UK Natural Environment Research Council National Capability programme CLASS (NE/R015953/1), NERC grants UK OSNAP (NE/K010875/1 and NE/K010875/2) and UK OSNAP Decade (NE/T00858X/1).

The authors thank the many scientists, officers and crew involved in the Ellett Array and Ellett Line cruises and shore-based analysis of the water samples. In particular, we thank Darren Rayner (NOC-Southampton) for designing and implementing the mooring array and Nicky Allison and her team (University of St Andrews) for their help with analyzing the carbon samples.

Open Research

Hydrographic section data from DY078, AR30-04 and DY120 are available from the British Oceanographic Data Centre (BODC) via doi:10.5285/0c3f44e7-8db9-04d5-e063-6c86abc0bc23, doi:10.5285/0814056c-7d07-248b-e063-6c86abc0dccf and doi:10.5285/0c665dcd-0bc9-6b5f-e063-6c86abc07096 respectively [*Clare Johnson*, 2023; 2024a; b].

Moored CTD and current meter data are available from BODC via https://www.bodc.ac.uk/data/bodc_database/nodb/data_collection/6550/ or via doi:10.5285/b8b40f85-8d3d-10c4-e053-6c86abc09e84 and doi:10.5285/cc3078f3-3008-4d6f-e053-6c86abc0ff6e [*Cunningham et al.*, 2023b; *Cunningham et al.*, 2021]. Collated data across all deployments are available from the SAMS thredds server at https://thredds.sams.ac.uk/thredds/catalog/osnap.html [*Cunningham et al.*, 2022].

Moored biogeochemical data can be requested manually from BODC or downloaded from the SAMS thredds server at https://thredds.sams.ac.uk/thredds/catalog/osnap.html [*Cunningham et al.*, 2022].

Volume and biogeochemical transports are available at https://thredds.sams.ac.uk/thredds/catalog/osnap.html [*Cunningham et al.*, 2023a].

Hydrographic section data from the Extended Ellett Line are available from BODC (https://www.bodc.ac.uk/data/bodc_database/nodb/data_collection/644/).

This study used E.U. Copernicus Marine Science Information GLORYSv1, doi:10.48670/moi-00021.

This work uses the software CO2SYSv3 for Matlab available at https://uk.mathworks.com/matlabcentral/fileexchange/78378-co2sysv3-for-matlab [*E Lewis and Wallace*, 1998; *Sharp et al.*, 2020; *van Heuven et al.*, 2011].

References

Alvarez, M., F. Perez, H. Bryden, and A. Rios (2004), Physical and biogeochemical transports structure in the North Atlantic subpolar gyre, *Journal of Geophysical Research: Oceans*, *109*, C03027, doi:doi:10.1029/2003JC002015.

Becker, S., M. Aoyama, E. Woodward, K. Bakker, C. S., C. Mahaffey, and T. Tanhua (2019), GO-SHIP Repeat Hydrography Nutrient Manual: The precise and accurate determination of dissolved inorganic nutrients in seawater, using Continuous Flow Analysis methods., in *GO-SHIP Repeat Hydrography Manual: A Collection of Expert Reports and Guidelines*, edited, p. 56 pp., doi:10.25607/OBP-555.

Bersch, M. (2002), North Atlantic Oscillation-induced changes of the upper-layer circulation in the northern North Atlantic, *Journal of Geophysical Research*, *107*(C10), Art. No. 3156.

Berx, B., et al. (2019), The observational potential of the transport mooring arrays: Assesment of the impact of upper-ocean measurements and of coherent integration of O_2 measurements for transport and fluxes in the Atlantic TMAs and synergies with the wider Atlantic observing system*Rep.*, 35 pp.

Binetti, U., J. Kaiser, G. Damerell, A. Rumyantseva, A. Martin, S. Henson, and K. Heywood (2020), Net community oxygen production derived from Seaglider deployments at the Porcupine Abyssal Plain site (PAP; northeast Atlantic) in 2012–13, *Progress in Oceanography*, *183*, doi:10.1016/j.pocean.2020.102293.

Bittig, H. C., T. Steinhoff, H. Claustre, B. Fiedler, N. L. Williams, R. Sauzède, A. Körtzinger, and J.-P. Gattuso (2018), An Alternative to Static Climatologies: Robust Estimation of Open Ocean CO2 Variables and Nutrient Concentrations From T, S, and O2 Data Using Bayesian Neural Networks, *Frontiers in Marine Science*, *5*, doi:10.3389/fmars.2018.00328.

Bostock, H. C., S. E. Mikaloff Fletcher, and M. J. M. Williams (2013), Estimating carbonate parameters from hydrographic data for the intermediate and deep waters of the Southern Hemisphere oceans, *Biogeosciences*, *10*(10), 6199-6213, doi:10.5194/bg-10-6199-2013.

Brown, P. J., et al. (2021), Circulation-driven variability of Atlantic anthropogenic carbon transports and uptake, *Nature Geoscience*, *14*(8), 571-577, doi:10.1038/s41561-021-00774-5.

Carracedo, L. I., H. Mercier, E. McDonagh, G. Rosón, R. Sanders, C. M. Moore, S. Torres-Valdés, P. Brown, P. Lherminier, and F. F. Pérez (2021), Counteracting Contributions of the Upper and Lower Meridional Overturning Limbs to the North Atlantic Nutrient Budgets: Enhanced Imbalance in 2010, *Global Biogeochemical Cycles*, *35*(6), e2020GB006898, doi:10.1029/2020GB006898.

Carter, B. R., H. C. Bittig, A. J. Fassbender, J. D. Sharp, Y. Takeshita, Y.-Y. Xu, M. Álvarez, R. Wanninkhof, R. A. Feely, and L. Barbero (2021), New and updated global empirical seawater property estimation routines, *Limnology and Oceanography: Methods*, *19*(12), 785-809, doi:10.1002/lom3.10461.

Carter, B. R., N. Williams, A. Gray, and R. Feely (2016), Locally interpolated alkalinity regression for global alkalinity estimation, *Limnology and Oceanography: Methods*, *14*, 268-277, doi:10.1002/lom3.10087.

Chaichana, S., T. Jickells, and M. Johnson (2019), Interannual variability in the summer dissolved organic matter inventory of the North Sea: implications for the continental shelf pump, *Biogeosciences*, *16*(5), 1073-1096, doi:10.5194/bg-16-1073-2019.

CMEMS (2022), GLORYS12v1 Global Ocean Physics Reanalysis [dataset], edited by E. U. C. M. S. I. C. M. D. S. (MDS). doi:10.48670/moi-00021.

Cunningham, S., M. Inall, K. Burmeister, L. Drysdale, E. Dumont, N. Fraser, C. Johnson, and S. Jones (2022), Rockall Trough hydrographic observations and transports from moorings and gliders [dataset], edited, https://thredds.sams.ac.uk/thredds/catalog/osnap.html.

Cunningham, S., M. Inall, K. Burmeister, L. Drysdale, E. Dumont, N. Fraser, C. Johnson, and S. Jones (2023a), Rockall Trough transports derived from moored observations. [dataset], edited, https://thredds.sams.ac.uk/thredds/catalog/osnap.html.

Cunningham, S., S. Jones, N. Holliday, E. Dumont, L. Drysdale, M. Inall, and D. Rayner (2023b), MicroCAT and current meter data from moorings of the Eastern Boundary array (Rockall Trough), funded by CLASS (Climate Linked Atlantic Sector Science), as a continuation of UK-OSNAP (Overturning in the Subpolar North Atlantic Programme) (2018-2020) [dataset], edited, NERC EDS British Oceanographic Data Centre NOC, doi:https://doi.org/10.5285/cc3078f3-3008-4d6f-e053-6c86abc0ff6e.

Cunningham, S., S. Jones, L. Houpert, E. Dumont, and M. Inall (2021), Microcat and current meter data from moorings of the Eastern Boundary array (Rockall Trough), as part of UK OSNAP (Overturning in the Subpolar North Atlantic Programme) (2017-2018) [dataset], edited, British Oceanographic Data Centre, National Oceanography Centre, NERC, UK, doi:https://doi.org/10.5285/b8b40f85-8d3d-10c4-e053-6c86abc09e84.

824 Daniels, C. J., A. J. Poulton, M. Esposito, M. L. Paulsen, R. Bellerby, M. St John, and A. P. Martin (2015),
825 Phytoplankton dynamics in contrasting early stage North Atlantic spring blooms: composition, succession, and
826 potential drivers, *Biogeosciences*, *12*(8), 2395-2409, doi:10.5194/bg-12-2395-2015.
827 Dickson, A., C. Sabine, and J. Christian (2007), Guide to best practises for ocean CO_2 measurements*Rep.*, 191 pp.
828 Fontela, M., H. Mercier, and F. Perez (2019), Long-term integrated biogeochemical budget driven by circulation in
829 the eastern subpolar North Atlantic, *Progress in Oceanography*, *173*, 51-65, doi:10.1016/j.pocean.2019.02.004.
830 Fox, A. D., et al. (2022), Exceptional freshening and cooling in the eastern subpolar North Atlantic caused by
831 reduced Labrador Sea surface heat loss, *Ocean Sci.*, *18*(5), 1507-1533, doi:10.5194/os-18-1507-2022.
832 Fransner, F., A. Olsen, M. Årthun, F. Counillon, J. Tjiputra, A. Samuelsen, and N. Keenlyside (2023),
833 Phytoplankton abundance in the Barents Sea is predictable up to five years in advance, *Communications Earth &*
834 *Environment*, *4*(1), 141, doi:10.1038/s43247-023-00791-9.
835 Fraser, N. J., et al. (2022), North Atlantic Current and European Slope Current Circulation in the Rockall Trough
836 Observed Using Moorings and Gliders, *Journal of Geophysical Research: Oceans*, *127*(12), e2022JC019291,
837 doi:10.1029/2022JC019291.
838 Gonzalez-Pola, C., K. M. H. Larsen, P. Fratantoni, and A. Beszczynska-Möller (2022), ICES Report on ocean
839 climate 2020*Rep.*, ICES Cooperative Research Reports (CRR).
840 Hansen, B., and S. Østerhus (2000), North Atlantic-Nordic Seas exchanges, *Progress in Oceanography*, *45*, 109-
841 208, doi:doi:10.1016/S0079-6611(99)00052-X.
842 Hartman, S. E., Z. P. Jiang, D. Turk, R. S. Lampitt, H. Frigstad, C. Ostle, and U. Schuster (2015), Biogeochemical
843 variations at the Porcupine Abyssal Plain sustained Observatory in the northeast Atlantic Ocean, from weekly to
844 inter-annual timescales, *Biogeosciences*, *12*(3), 845-853, doi:10.5194/bg-12-845-2015.
845 Hátún, H., et al. (2017), The subpolar gyre regulates silicate concentrations in the North Atlantic, *Scientific Reports*,
846 *7*(1), 14576, doi:10.1038/s41598-017-14837-4.
847 Hátún, H., A. Sandø, H. Drange, B. Hansen, and H. Valdimarsson (2005), Influence of the Atlantic Subpolar Gyre
848 on the Thermohaline Circulation, *Science*, *309*, 19841-11844, doi:doi:10.1126/science.1114777
849 Heath, M. R., and D. J. Beare (2008), New primary production in northwest European shelf seas, 1960–2003,
850 *Marine Ecology Progress Series*, *363*, 183-203, doi:10.3354/meps07460.
851 Henson, S., R. Lampitt, and D. Johns (2012), Variability in phytoplankton community structure in response to the
852 North Atlantic Oscillation and implications for organic carbon flux, *Limnology and Oceanography*, *57*(6), 1591-
853 1601, doi:10.4319/lo.2012.57.6.1591.
854 Holliday, N. P., et al. (2020), Ocean circulation causes the largest freshening event for 120 years in eastern subpolar
855 North Atlantic, *Nature Communications*, *11*(1), 585, doi:10.1038/s41467-020-14474-y.
856 Holliday, N. P., et al. (2008), Reversal of the 1960s to 1990s freshening trend in the northeast North Atlantic and
857 Nordic Seas, *Geophysical Research Letters*, *35*(3), doi:10.1029/2007GL032675.
858 Holt, J., M. Butenschön, S. L. Wakelin, Y. Artioli, and J. I. Allen (2012), Oceanic controls on the primary
859 production of the northwest European continental shelf: model experiments under recent past conditions and a
860 potential future scenario, *Biogeosciences*, *9*(1), 97-117, doi:10.5194/bg-9-97-2012.
861 Houpert, L., S. Cunningham, N. Fraser, C. Johnson, N. P. Holliday, S. Jones, B. Moat, and D. Rayner (2020),
862 Observed Variability of the North Atlantic Current in the Rockall Trough From 4 Years of Mooring Measurements,
863 *Journal of Geophysical Research: Oceans*, *125*(10), e2020JC016403, doi:10.1029/2020JC016403.
864 Houpert, L., M. E. Inall, E. Dumont, S. Gary, C. Johnson, M. Porter, W. E. Johns, and S. A. Cunningham (2018),
865 Structure and Transport of the North Atlantic Current in the Eastern Subpolar Gyre From Sustained Glider
866 Observations, *Journal of Geophysical Research: Oceans*, *123*(8), 6019-6038, doi:10.1029/2018JC014162.
867 Hu, Y. (2022), Temperature coefficient of seawater pH as a function of temperature, pH, DIC and salinity, *Acta*
868 *Oceanologica Sinica*, *41*, 114-118, doi:10.1007/s13131-021-1955-3.
869 Humphreys, M., et al. (2019), Mechanisms for a nutrient-conserving carbon pump in a seasonally stratified,
870 temperate continental shelf sea, *Progress in Oceanography*, *177*, doi:10.1016/j.pocean.2018.05.001.
871 Huthnance, J., et al. (2022), Ocean shelf exchange, NW European shelf seas: Measurements, estimates and
872 comparisons, *Progress in Oceanography*, *202*, doi:10.1016/j.pocean.2022.102760.
873 Johnson, C. (2023), Hydrographic section data (dissolved inorganic nutrients, dissolved inorganic carbon and total
874 alkalinity) from AR30-04 from the Eastern Boundary array (Rockall Trough), as part of UK OSNAP (Overturning
875 in the Subpolar North Atlantic Programme) [dataset], edited, NERC EDS British Oceanographic Data Centre NOC,
876 doi:https://doi.org/10.5285/0814056c-7d07-248b-e063-6c86abc0dccf.
877 Johnson, C. (2024a), Hydrographic section data (dissolved inorganic nutrients, dissolved inorganic carbon and total
878 alkalinity) from DY078, May 2017, from the Eastern Boundary array (Rockall Trough), as part of UK OSNAP

(Overturning in the Subpolar North Atlantic Programme) [dataset], edited, NERC EDS British Oceanographic Data Centre NOC, doi:https://doi.org/10.5285/0c3f44e7-8db9-04d5-e063-6c86abc0bc23.
Johnson, C. (2024b), Hydrographic section data (dissolved inorganic nutrients, dissolved inorganic carbon and total alkalinity) from DY120, October 2020, from the Eastern Boundary array (Rockall Trough) and Iceland Basin, as part of UK OSNAP (Overturning in the Subpolar North Atlantic Programme) [dataset], edited, NERC EDS British Oceanographic Data Centre NOC, doi:https://doi.org/10.5285/0c665dcd-0bc9-6b5f-e063-6c86abc07096.
Johnson, C., M. Inall, and S. Häkkinen (2013), Declining nutrient concentrations in the northeast Atlantic as a result of a weakening Subpolar Gyre, *Deep Sea Research I*, *82*, 95-107, doi:doi:10.1016/j.dsr.2013.08.007.
Johnson, K. S., et al. (2017), Biogeochemical sensor performance in the SOCCOM profiling float array, *Journal of Geophysical Research: Oceans*, *122*(8), 6416-6436, doi:10.1002/2017JC012838.
Jones, S., F. Cottier, M. Inall, and C. Griffiths (2018), Decadal variability on the Northwest European continental shelf, *Progress in Oceanography*, *161*, 131-151, doi:org/10.1016/j.pocean.2018.01.012.
Jones, S., M. Inall, M. Porter, J. A. Graham, and F. Cottier (2020), Storm-driven across-shelf oceanic flows into coastal waters, *Ocean Sci.*, *16*(2), 389-403, doi:10.5194/os-16-389-2020.
Juranek, L. (2022), Changing Biogeochemistry of the Arctic Ocean: Surface Nutrient and CO2 Cycling in a Warming, Melting North, *Oceanography*, *35*, 144-155, doi:10.5670/oceanog.2022.120.
Jutras, M., C. O. Dufour, A. Mucci, and L. C. Talbot (2023), Large-scale control of the retroflection of the Labrador Current, *Nature Communications*, *14*(1), 2623, doi:10.1038/s41467-023-38321-y.
Koman, G., W. Johns, A. Houk, L. Houpert, and F. Li (2022), Circulation and overturning in the eastern North Atlantic subpolar gyre, *Progress in Oceanography*, *208*, doi:10.1016/j.pocean.2022.102884.
Koul, V., C. Schrum, A. Düsterhus, and J. Baehr (2019), Atlantic Inflow to the North Sea Modulated by the Subpolar Gyre in a Historical Simulation With MPI-ESM, *Journal of Geophysical Research: Oceans*, *124*(3), 1807-1826, doi:10.1029/2018JC014738.
Langdon, C. (2010), Determination of dissolved oxygen in seawater by winkler titration using the amperometric technique, in *GO-SHIP Repeat Hydrography Manual: A Collection of Expert Reports and Guidelines*, edited, p. 18 pp., doi:10.25607/OBP-1350.
Lavin, A., H. Bryden, and G. Parrilla (2003), Mechanisms of heat, freshwater, oxygen and nutrient transports and budgets at 24.5°N in the subtropical North Atlantic, *Deep Sea Research*, *50*, 1099-1128, doi:10.1016/S0967-0637(03)00095-5.
Lewis, E., and D. Wallace (1998), Program developed for CO2 system calculations [software]*Rep.*, 38 pp, https://www.ncei.noaa.gov/access/ocean-carbon-acidification-data-system/oceans/CO2SYS/co2rprt.html.
Lewis, K. M., G. L. van Dijken, and K. R. Arrigo (2020), Changes in phytoplankton concentration now drive increased Arctic Ocean primary production, *Science*, *369*(6500), 198-202, doi:10.1126/science.aay8380.
Lozier, M., et al. (2019), A sea change in our view of overturning in the subpolar North Atlantic, *Science*, *363*, 516-521, doi:doi:10.1126/science.aau6592.
Marsh, B., I. Haigh, S. Cunningham, M. Inall, M. Porter, and B. Moat (2017), Large-scale forcing of the European Slope Current and associated inflows to the North Sea, *Ocean Science*, *13*, 315-335, doi:doi:10.5194/os-13-315-2017.
Martinez, E., D. Antoine, F. D'Ortenzio, and C. de Boyer Montégut (2011), Phytoplankton spring and fall blooms in the North Atlantic in the 1980s and 2000s, *Journal of Geophysical Research: Oceans*, *116*(C11), doi:10.1029/2010JC006836.
Maze, G., H. Mercier, V. Thierry, L. Memery, P. Morin, and F. F. Perez (2012), Mass, nutrient and oxygen budgets for the northeastern Atlantic Ocean, *Biogeosciences*, *9*(10), 4099-4113, doi:10.5194/bg-9-4099-2012.
Oziel, L., G. Neukermans, M. Ardyna, C. Lancelot, J.-L. Tison, P. Wassmann, J. Sirven, D. Ruiz-Pino, and J.-C. Gascard (2017), Role for Atlantic inflows and sea ice loss on shifting phytoplankton blooms in the Barents Sea, *Journal of Geophysical Research: Oceans*, *122*(6), 5121-5139, doi:10.1002/2016JC012582.
Pätsch, J., V. Gouretski, I. Hinrichs, and V. Koul (2020), Distinct Mechanisms Underlying Interannual to Decadal Variability of Observed Salinity and Nutrient Concentration in the Northern North Sea, *Journal of Geophysical Research: Oceans*, *125*(5), e2019JC015825, doi:10.1029/2019JC015825.
Pelegrí, J. L., and G. T. Csanady (1991), Nutrient transport and mixing in the Gulf Stream, *Journal of Geophysical Research: Oceans*, *96*(C2), 2577-2583, doi:10.1029/90JC02535.
Porter, M., A. Dale, S. Jones, B. Siemering, and M. Inall (2018), Cross-slope flow in the Atlantic Inflow Current driven by the on-shelf deflection of a slope current, *Deep Sea Research*, *140*, 173-185, doi:10.1016/j.dsr.2018.09.002.

933 Proctor, R., J. Holt, J. Allen, and J. Blackford (1993), Nutrient fluxes and budgets for the North West European
934 Shelf from a three-dimensional model, *The Science of the Total Environment*, *314-316*, 769-785,
935 doi:10.1016/S0048-9697(03)00083-4.
936 Rey, F. (2012), Declining silicate concentrations in the Norwegian and Barents Seas, *ICES Journal of Marine*
937 *Science*, *69*(2), 208-212, doi:10.1093/icesjms/fss007.
938 Robbins, P., and H. Bryden (1994), Direct observations of advective nutrient and oxygen fluxes at 24°N in the
939 Pacific Ocean, *Deep Sea Research*, *41*, 143-168, doi:10.1016/0967-0637(94)90030-2.
940 Sharp, J., D. Pierrot, M. Humphreys, J. Epitalon, J. Orr, E. Lewis, and D. Wallace (2020), CO2SYSv3 for MATLAB
941 [software], edited, https://doi.org/10.5281/ZENODO.3950563.
942 Tanhua, T., P. Brown, and R. Key (2009), CARINA: nutrient data in the Atlantic Ocean, *Earth Systems Science*
943 *Data*, *1*, 7-24.
944 Thomas, H., Y. Bozec, K. Elkalay, and H. de Baar (2004), Enhanced open ocean storage of CO2 from shelf sea
945 pumping, *Science*, *14*, 1005-1008, doi:10.1126/science.1095491.
946 Torres-Valdés, S., T. Tsubouchi, S. Bacon, A. C. Naveira-Garabato, R. Sanders, F. A. McLaughlin, B. Petrie, G.
947 Kattner, K. Azetsu-Scott, and T. E. Whitledge (2013), Export of nutrients from the Arctic Ocean, *Journal of*
948 *Geophysical Research: Oceans*, *118*(4), 1625-1644, doi:10.1002/jgrc.20063.
949 Tuerena, R. E., et al. (2022), Nutrient pathways and their susceptibility to past and future change in the Eurasian
950 Arctic Ocean, *Ambio*, *51*(2), 355-369, doi:10.1007/s13280-021-01673-0.
951 van Heuven, S., D. Pierrot, J. Rae, E. Lewis, and D. Wallace (2011), Matlab program developed for CO2 system
952 calculations [software]*Rep.*, https://doi.org/10.3334/CDIAC/otg.CO2SYS_MATLAB_v1.1.
953 Wassmann, P., et al. (2006), Food webs and carbon flux in the Barents Sea, *Progress in Oceanography*, *71*, 232-
954 287, doi:10.1016/j.pocean.2006.10.003.
955 Wei, X., J. Hopkins, M. Oltmanns, C. Johnson, and M. Inall (in press), The role of deep winter mixing and wind-
956 driven surface Ekman transport in supplying oceanic nitrate to a temperate shelf sea, *Journal of Geophysical*
957 *Research: Oceans*.
958 Williams, R. G., E. McDonagh, V. M. Roussenov, S. Torres-Valdes, B. King, R. Sanders, and D. A. Hansell (2011),
959 Nutrient streams in the North Atlantic: Advective pathways of inorganic and dissolved organic nutrients, *Global*
960 *Biogeochemical Cycles*, *25*(4), doi:10.1029/2010GB003853.
961 Zunino, P., P. Lherminier, H. Mercier, X. A. Padín, A. F. Ríos, and F. F. Pérez (2015), Dissolved inorganic carbon
962 budgets in the eastern subpolar North Atlantic in the 2000s from in situ data, *Geophysical Research Letters*, *42*(22),
963 9853-9861, doi:10.1002/2015GL066243.
964